Thesis for the degree of Licentiate of Engineering

Remote sensing of clouds and precipitation using active and passive microwave observations

Simon Pfreundschuh

Department of Space, Earth and Environment
CHALMERS UNIVERSITY OF TECHNOLOGY
Göteborg, Sweden 2019

Remote sensing of clouds and precipitation using active and passive microwave observations
Simon Pfreundschuh

Department of Space, Earth and Environment
Chalmers University of Technology
SE–412 96 Göteborg, Sweden
Telephone + 46 (0) 31 – 772 1000

Cover: Co-located observations of a convective cloud system in the Coral Sea. Optical observations from the MODIS sensor are displayed as true-color composite on the surface. Contours show the isolines of the passive microwave radiances measured by the GMI sensor. The vertical transect shows radar reflectivities measured by the CloudSat CPR.

Typeset by the author using LaTeX.

Printed by Chalmers Reproservice
Göteborg, Sweden 2019

Gosto de um modo carinhoso do inacabado, do malfeito, daquilo que desajeitadamente tenta um pequeno vôo e cai sem graça no chão.

— Clarice Lispector

Remote sensing of clouds and precipitation using active and passive microwave observations

Thesis for the degree of Licentiate of Engineering

Simon Pfreundschuh
Department of Space, Earth and Environment
Chalmers University of Technology

Abstract

Global observations of clouds and precipitation are of great importance for weather prediction and the monitoring of the climate. Nonetheless, the currently available record of global observations does not constrain the properties of clouds very well owing to the inherent limitations of the observation systems used to produce them. The upcoming Ice Cloud Imager (ICI) microwave radiometer, which will be launched on the next generation of European weather satellites, will improve this situation by providing observations of clouds at sub-millimeter wavelengths. ICI will be the first sensor of its kind to deliver these observations, which will significantly improve the sensitivity to small ice particles and low mass concentrations compared to currently available microwave observations.

This thesis presents research aimed at developing knowledge and methodology required for the modeling and interpretation of the observations that will be provided by ICI. Two studies are presented which propose a method for measuring distributions of ice hydrometeors from ICI-type sub-millimeter observations combined with radar observations.

The first study uses simulated observations to assess the potential benefits of combining sub-millimeter radiometer observations with radar observations for the retrieval of ice hydrometeors. It is found that the combined observations improve the sensitivity to microphysical properties of clouds, which can help to reduce the error in the retrieved mass concentrations for specific hydrometeor types. Furthermore, improved sensitivity to supercooled liquid cloud is found as an additional synergy between the active and passive observations.

The second study aims to validate the results from the first by applying the synergistic retrieval algorithm to observations from a flight campaign. The retrieval algorithm is found to show overall good agreement with in-situ measured ice concentrations taking into account the sensitivity limits of the sensors. In addition to that, indications of a signal from mixed-phase particles are found in observations of convective updrafts.

In the two presented studies, a synergistic retrieval algorithm for ice hydrometeors from radar and passive sub-millimeters has been developed, characterized and validated. The method can be applied in a future satellite mission to reduce uncertainties in global observations of clouds or used to study cloud microphysical properties in field campaigns. In addition to that, the presented application to field campaign data provides one of the rare validation cases for the radiative transfer modeling involving clouds at sub-millimeter wavelengths.

Keywords: Microwave remote sensing, hydrometeors, clouds, precipitation

Acknowledgments

First of all, I would like to thank my supervisor Patrick Eriksson for his supervision and guidance during these first two-and-a-half years of my research. For sharing his knowledge on remote sensing and radiative transfer as well as reminding me that there is more to remote sensing than just the Mathematics.

David Duncan, my co-supervisor, for his advice and inspiring discussions on remote sensing, atmospheric processes and beyond. For long runs and even longer bike rides.

Prof. Stefan A. Buehler, Dr. Manfred Brath and Oliver Lemke from the University of Hamburg for the collaboration on ARTS as well as for always finding some space for me when I am in Hamburg.

My present and former colleagues from the Division of Microwave and Optical Remote Sensing for their continuous feedback and support. Especially, I would like to thank Donal Murtagh, Vasileios Barlakas, Robin Ekelund and of course Patrick Eriksson for reading through this thesis and providing valuable feedback even on short notice.

Julia Kukulies for her feedback on this thesis and the courage required to produce it.

Simon Pfreundschuh
Göteborg, November 2019

List of Publications

This thesis is based on the following appended papers:

Paper 1. Pfreundschuh, S., Eriksson, P., Buehler, S. A., Brath, M., Duncan, D., Larsson, R., and Ekelund, R. (2019). "Synergistic radar and radiometer retrievals of ice hydrometeors ", Atmos. Meas. Tech. Discuss., in review.

Paper 2. Pfreundschuh, S., Eriksson, P., Buehler, S. A., Brath, M., Duncan, D., Ewald, F., and Delanoë, J. (2019). "Relating microphysical and radiometric properties of cloud hydrometeors at millimeter and sub-millimeter wavelengths", Atmos. Meas. Tech. Discuss., manuscript in preparation.

Other relevant publications authored or co-authored by Simon Pfreundschuh:

Ekelund, R., Eriksson, P., and Pfreundschuh, S. (2019). "Using passive and active microwave observations to constrain ice particle models", Atmos. Meas. Tech. Discuss, in review.

Hagen, J., Hocke, K., Stober, G., Pfreundschuh, S., Murk, A., and Kämpfer, N. (2019). "First measurements of tides in the stratosphere and lower mesosphere by ground-based Doppler microwave wind radiometry", Atmos. Chem. Phys. Discuss., in review.

Duncan, D. I., Eriksson, P., and Pfreundschuh, S. (2019). "An experimental 2DVAR retrieval using AMSR2", Atmos. Meas. Tech. Discuss., accepted.

Duncan, D. I., Eriksson, P., Pfreundschuh, S., Klepp, C., and Jones, D. C. (2019). "On the distinctiveness of observed oceanic raindrop distributions", Atmos. Chem. Phys., 19, 6969–6984, https://doi.org/10.5194/acp-19-6969-2019.

Pfreundschuh, S., Eriksson, P., Duncan, D., Rydberg, B., Håkansson, N., and Thoss, A (2018). "A neural network approach to estimating a posteriori distributions of Bayesian retrieval problems", Atmos. Meas. Tech. , 11, 4627–4643, https://doi.org/10.5194/amt-11-4627-2018.

Contents

Part I

Introductory chapters

Chapter 1

Introduction

Clouds and precipitation affect life on Earth in various ways and on multiple time scales. On short time scales, weather affects human activity, potentially posing threats to transport, agriculture and lifes. On longer time scales, precipitation patterns shape ecosystems and societies while clouds influence the global climate by means of their interaction with the incoming and outgoing electromagnetic radiation.

Understanding and predicting weather and climate has been a human endeavor dating back at least to the formation of the first settled communities during the agricultural revolution (Hellmann 1908). This is easily understood considering the dependence of agricultural activity on benign weather patterns. Today, this dependency may have even increased as more and more branches of human activity rely on the availability of accurate weather forecasts.

With the dramatic effects of anthropogenic climate change becoming more and more apparent (Coronese et al. 2019; Grinsted et al. 2019), it is indisputable that a firm understanding of the Earth's climate system is critical to ensure a safe passage into this uncertain future. The predicted heating under all but the lowest emission scenarios is likely to exceed 2 °C by the end of the century (Collins et al. 2013). With this, global mean surface air temperature will likely surpass even the highest temperatures found in reconstructions of past climate (Masson-Delmotte et al. 2013). To ensure effective adaptation to these drastic changes, comprehensive observation and modeling of the Earth's climate is indispensable.

The subject of this thesis are observational methods for clouds and precipitation using microwave radiation. These observations provide a monitoring system for the climate on Earth and are crucial ingredients in today's weather forecasting systems. In addition to this, they provide a reference for the evaluation and improvement of climate models. More specifically, the research presented here focuses on observations of clouds at sub-millimeter wavelengths. Such observations will become available with the upcoming second generation of European operational weather satellites (Metop-SG). The aim of the presented research is to develop the methodology and know-how, which is necessary to make effective use of these novel observations. The two presented projects focus on the combination of observations from passive sub-millimeter radiometers with those from a radar and the question how these can be used to more accurately determine the properties of clouds.

The remainder of this section provides an overview over the relevance of observations of clouds for both weather and climate applications and closes with a discussion of currently available observation methods. The following chapters then provide an introduction to the physical and mathematical principles upon which these observations are founded. Chapter 2 provides an introduction to cloud formation and establishes what properties of clouds can be observed. Chapter 3 introduces the theory of radiative transfer which is necessary to understand the observable effects that clouds have on microwave radiation. Chapter 4 introduces the mathematical methods that are used to infer relevant properties of clouds from remote sensing observations.

A brief note on the terminology: The term "hydrometeor" will be used frequently in the following chapter to denote the aqueous particles that make up clouds and precipitation. Moreover, the viewpoint adopted here is that precipitation is a byproduct of cloud formation and therefore the terms *observations of clouds* or *cloud observations* are used to denote observations of both clouds and, if present, precipitation.

1.1 The role of clouds and precipitation in numerical weather prediction

Clouds and precipitation are responsible for many of the phenomena that are considered as weather. The most prominent example for this are certainly storms which can bring strong winds and heavy precipitation. It is clear that accurate representation clouds in numerical weather prediction (NWP) models is an essential requirement for reliable forecasts. But clouds, more specifically observations of clouds, can impact weather forecasts in another, more nuanced way.

The forecasting systems which are used to generate weather forecasts make use of satellite observations to determine an optimal initial state from which a forecast run is started. This process is called data assimilation. In a clear atmosphere, satellite observations from infrared and microwave sensors provide direct information on the temperature and humidity field of the atmosphere. By assimilating observations over multiple time steps, these observation can provide additional information on the dynamical state of the atmosphere (Geer et al. 2018).

Clouds form where warm and moist air is transported upwards in the atmosphere. Because of this relation to the dynamics of the atmosphere, clouds act as a tracer from which a data assimilation system can extract valuable information on the state of the atmosphere. Indeed, owing to recent developments in data assimilation methodology, microwave observations sensitive to humidity and clouds have become a main contributor to short-term forecast skill (Geer et al. 2017).

1.2 The role of clouds and precipitation in the climate system

Clouds are an integral part of the global hydrological cycle in which they deliver water from the atmosphere to the surface of the Earth. They are also tightly coupled to the dynamics of the atmosphere through the effects of latent heat and the modulation of atmospheric heating profiles (Bony et al. 2015). Their principal impact on the climate system, however, is through their interaction with the incoming solar radiation and the outgoing long-wave radiation.

1.2.1 The global energy budget

The short-wave radiation emitted by the sun that reaches the earth is the energy source that drives the climate system. To remain at a stable temperature, the Earth needs to emit the same amount of incoming energy in the form of outgoing long-wave radiation. From an energy balance perspective, clouds have two opposing effects on the global energy budget: Firstly, a cooling effect caused by the reflection of incoming short-wave radiation back to space, and secondly, a warming effect caused by the blocking of outgoing long-wave radiation that would be emitted to space in a cloud-free atmosphere. Overall, the reflection of incoming sunlight dominates, so that clouds exercise a net cooling effect on the climate system.

1.2.2 Cloud radiative effect and climate sensitivity

Since both the cooling and warming effects of clouds are relatively strong, changes in cloud properties or occurrence have the potential to cause significant feedbacks in a changing climate. These effects, however, are difficult to quantify. This is because the strength and the type of the interaction between clouds and the incoming or outgoing radiation depends on where these clouds form in the atmosphere. In addition to this, they are affected also by the microphysical properties of the cloud, e.g. particle shape, phase and size distribution.

An additional difficulty in representing the effect of clouds in the general circulation models (GCMs) that are used for climate prediction is that their formation and evolution involves processes at size-ranges beginning at the nanometer scales of aerosol particles on which cloud drops form up to several thousands of kilometers, which is the size of synoptic-scale cyclones. Since such a range of size-scales cannot be represented explicitly in a GCM, models have to rely on approximate representations of cloud processes.

Regarding predictions of future climate, it is indeed the strength of feedback effects involving clouds that exhibit the largest spread between different models. Clouds are therefore recognized as one of the major sources of uncertainty in current climate models and contribute significantly to the spread in predicted changes of global mean surface temperature that is observed between different GCMs (Boucher et al. 2013).

1.3 Global observations of clouds

The two previous sections described the relevance of cloud observations for weather and climate applications. From this we now turn to a brief review of currently available observation methods for clouds. The focus here is on satellite-based systems, since these are the only ones that can simultaneously provide observations at global scale and sufficiently high temporal sampling.

1.3.1 Frequency domains

Hydrometeors can be observed from the optical domain down to microwave frequencies around 10 GHz. The strength of their interaction with radiation depends on the relation of their size to the wavelength of the radiation. The interaction is strongest when the wavelength is close to the size of the particles.

In the optical domain, cloud droplets and ice crystals are large compared to the wavelength of the radiation, which is why they efficiently scatter of radiation at these wavelengths. The high number concentrations of these particles present in clouds make most of them opaque. For observations in the infrared, the wavelength approaches the size of the smallest hydrometeors around 5 μm. Since this further increases the strength of the interaction between the cloud particles of the radiation, clouds become even more opaque at these frequencies.

This has important implications for cloud observations using optical or infrared radiation. Due to the opacity of most clouds, the observed radiation is sensitive only to the upper-most regions of the cloud. Observational techniques based on these wavelengths have therefore no direct sensitivity to precipitation and large parts of the mass of thick clouds.

At microwave frequencies, the wavelength of the radiation is much larger than the size of the hydrometeors, which renders it insensitive to all but the largest hydrometeors. The advantage of microwave observations, however, is that they can directly sense precipitation, which occurs at the base of and below clouds that are too thick for optical or infrared radiation to penetrate.

An example of this is given in Fig. 1.1, which shows simultaneous observations of a tropical cloud system in the optical and the microwave domain. Each panel shows a true-color composite overlaid with the isolines of microwave observations at different wavelengths. Considering the lowest microwave frequency (Panel (a)), 10 GHz, it can be seen that the microwave observation exhibits structure in those regions where the optical image is saturated, i.e. only the white cloud top is visible. As the frequency increases (Panel (b) and (c)), the structures observed in microwave image become more complex, since the sensitivity of the radiation to hydrometeors as well as water vapor increases. At 183 GHz (Panel (d)), the sensitivity to atmospheric humidity is so large that the radiation cannot sense the lower troposphere anymore. A signal from the cloud is therefore only observed where it reaches high enough altitudes for its ice particles to scatter the up-welling thermal radiation. We will turn back to this scene for a more detailed discussion of the observable effects of clouds and

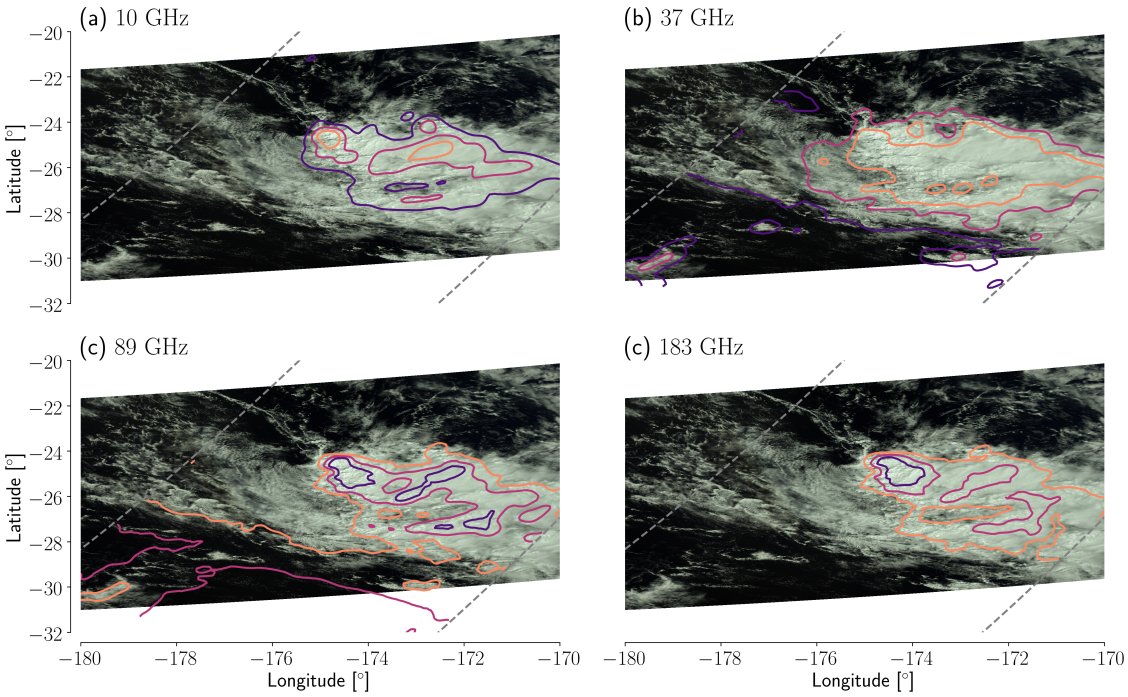

Figure 1.1: The background image in each panel shows true-color composites of observations from the MODIS sensor. Plotted on top are the contours of the radiances of different channels of the GMI (Draper et al. 2015) radiometer. Dashed, gray lines mark the boundaries of the GMI swath.

precipitation on microwave radiation in Chapter 3, which explains the principles of radiative transfer in the presence of clouds and precipitation.

1.3.2 Active and passive sensors

So far, only observations from passive sensors have been discussed. Passive sensors are sensors that measure the radiation emitted by the sun or the earth system. The signal observed by passive sensors at wavelengths shorter than 5 μm is dominated by sunlight that was scattered or reflected by the Earth or its atmosphere. At longer wavelengths, i.e. in the thermal infrared and microwave regions of the electromagnetic spectrum sensors measure the thermal emission from the Earth's surface or atmosphere.
In contrast to this, active sensors emit radiation themselves and measure the amount of if that is reflected back to the sensor. The two types of active sensors that are relevant for studying clouds are radars and lidars. The main difference between radar and lidars are the frequencies at which they operate: While a radar uses microwaves, lidars operate at infrared, optical or UV wavelengths. The advantage of active sensors is that they can provide vertically resolved observations and generally have greater sensitivity than their passive counterparts. The vertical resolution, however, generally comes at the cost of a decreased horizontal coverage. Active sensors therefore typically provide significantly lower temporal sampling of specific locations on Earth than their passive counterparts.
As an example for observations from an active sensor, radar observations of the

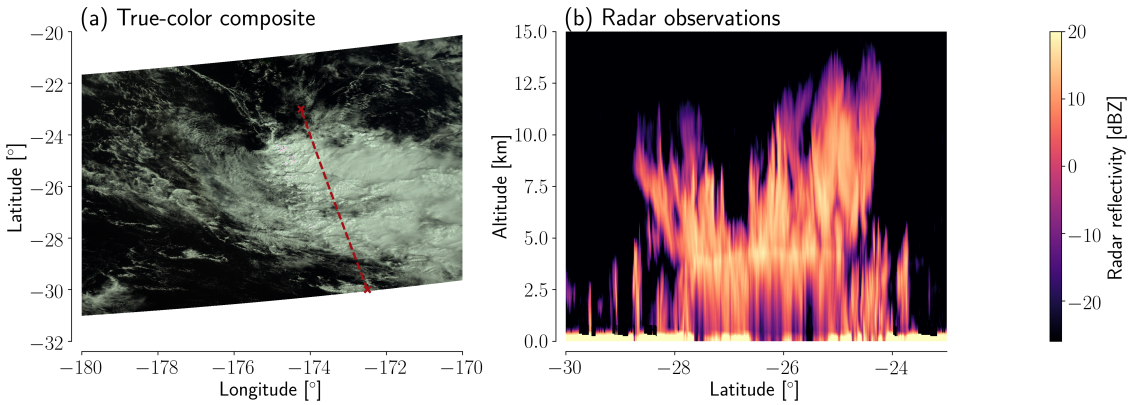

Figure 1.2: Radar observations of the tropical cloud system shown in Fig. 1.1. Panel (a) displays once again the observations from the optical domain together with the ground track of the radar observations (dashed, red line). Panel (b) displays the radar reflectivities observed by the Cloud Profiling Radar on the CloudSat satellite (Tanelli et al. 2008) along the track marked in Panel (a).

tropical scene considered above are displayed in Fig. 1.2. Shown in Panel (a) of the figure are once again the passive observations in the optical together with the ground track of the radar observations. The radar observations along the ground track are displayed in Panel (b) of the figure. The radar observations nicely reveal the intricate vertical structure of the cloud. In the northernmost part of the cloud system, the cloud reaches up to altitudes of almost 15 km, a sign of strong convective activity. Moreover, a radar signal that reaches down to the surface is observed almost everywhere in the cloud, indicating the presence of precipitation.

1.3.3 A look into the future

There is a considerable gap in the available wavelengths for the observations of clouds between the shortest microwave wavelengths around 2 mm and the longest infrared wavelength at around 15 μm. This gap is partly due to the strength of the water vapor continuum in this region of the electromagnetic spectrum, which effectively makes the troposphere invisible for large parts of the range, as well as technological difficulties in the development of sensors for these wavelengths.
Nonetheless, progress is underway to narrow down this wavelength gap. The Ice Cloud Imager (ICI, Buehler et al. (2012)) is a new type of sensor that will be flown on the upcoming second generation of European operational meteorological satellites (Metop-SG). It will provide observations of the atmosphere at frequencies up to 664 GHz corresponding to a wavelength of less than 0.5 mm. These observations at sub-millimeter wavelengths will considerably increase the sensitivity to small particles and lower hydrometeor masses. Moreover, ICI is expected to also provide increased sensitivity to the shape of ice particles.
Since ICI will be the first sensor of its kind to provide observations of clouds at sub-millimeter wavelengths, the development of new methodology and know-how is required to fully exploit their potential. ICI's sensitivity to the microphysical properties of hydrometeors requires improvements of their representation in radiative

transfer models and better knowledge of their characteristic distribution in the atmosphere to accurately simulate and understand the impact of ice particles on sub-millimeter observations. Contributing to these preparations for the ICI sensor are the principal aims of the research project that led to this thesis.

Chapter 2

The physics of clouds and precipitation

Clouds consist of large numbers of water droplets and ice crystals that are suspended in the air. When these drops grow sufficiently in mass they eventually fall out of the cloud to form precipitation. This chapter gives an overview over the processes that lead to the formation of clouds and ultimately precipitation. Moreover, the typical properties of the hydrometeors that make up clouds and precipitation are presented. This knowledge is required to understand the capabilities and limitations of the observational approaches considered in the remainder of this thesis. The presentation given below is based on the book by Lohmann et al. (2016).
The discussion of clouds presented here focuses on their microphysical properties and therefore distinguishes between warm and cold clouds. Warm clouds exist below the 0 °C isotherm and consist solely of liquid water droplets. Cold clouds extend above the 0 °C isotherm and consist at least in part of ice particles. Although, typically, the liquid phase is present also in cold clouds, this classification allows the slightly different formation processes of liquid and frozen hydrometeors to be discussed separately. Although it is common to further classify clouds according to their structure and the dynamical context of their formation, this only indirectly affects their interaction with radiation and is therefore neglected here.
This chapter begins with a brief overview over the different hydrometeor types and sizes present in clouds. Thereafter, phase transitions are introduced which form the basis of cloud formation processes. This is followed by a description of the formation and growth processes in warm and cold clouds. The chapter closes with a brief discussion of the general properties of precipitation.

2.1 Types of hydrometeors

Liquid cloud droplets form through the activation of solution droplets, which are aerosols that have taken up humidity from their environment. The typical sizes of cloud droplets range from 5 μm to 20 μm and they are the smallest particles that can be found in tropospheric clouds. If cloud droplets grow by colliding with other cloud droplets they eventual become drizzle drops, which have typical sizes starting

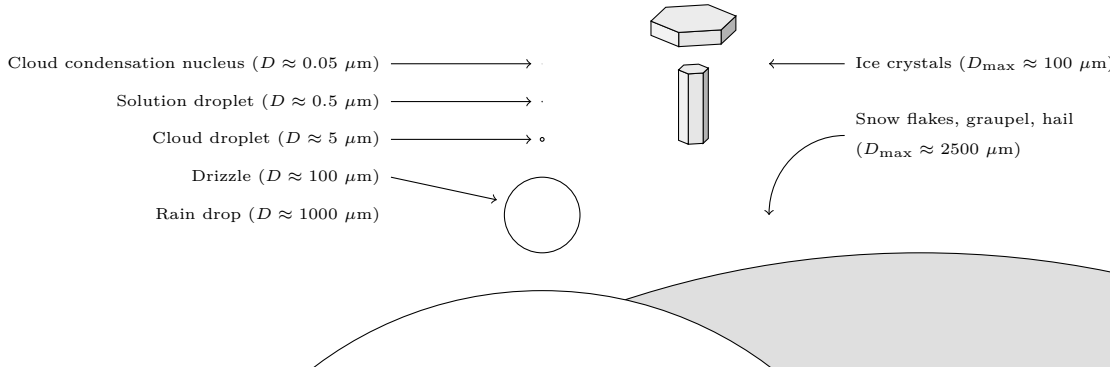

Figure 2.1: Types of hydrometeors and their sizes. The figure schematically displays the different particles formed inside clouds. The particles are drawn to scale with an enlargement factor of 1000.

from 100 μm and are heavy enough to fall out of the cloud and reach the ground. When sufficiently many other droplets are available, drizzle droplets can continue to grow to form rain drops which have sizes from 1 to about 4 mm.

Ice crystals are the frozen counterpart to cloud droplets and typically have sizes around 100 μm but can become significantly larger and even fall out of the cloud to reach the ground. Graupel is created when ice crystals collide with cloud droplets that freeze upon the ice crystal. This process is called riming. When an ice crystal grows to sizes larger than 2.5 mm through riming it is called a hailstone (Ch. 11, Lohmann et al. (2016)). Snow flakes consist of aggregates of ice crystals and range in sizes from millimeters to centimeters.

The different types of hydrometeors and their respective sizes are summarized in Fig. 2.1. It should be noted that the size given in the figure as well as the above paragraphs are only indications of size range corresponding to each particle type. Their exact sizes can vary greatly from particle to particle and from cloud to cloud.

2.2 The physics of cloud formation

Cloud hydrometeors form when water vapor contained in the air undergoes a phase change from the gas phase to the liquid or frozen phase. This process is denoted as condensation, for the change from the gas to the liquid phase, and deposition, for the change from the gas to the ice phase.

A necessary condition for condensation to occur is that the air is supersaturated with respect to liquid water. This means that the partial pressure of water vapor exceeds the saturation vapor pressure with respect to liquid water. Similarly, supersaturation with respect to the ice phase is required for the formation of ice particles. The supersaturation required for cloud formation is reached when comparably warm and moist air is lifted in the atmosphere. The resulting adiabatic cooling of the air leads

to a decrease in the saturation vapor pressures of water and ice and the air eventually becomes supersaturated.
When water vapor reaches supersaturation with respect to either the liquid or ice phase it enters a metastable state. This means that although the liquid state is energetically favorable the transition is inhibited by an energy barrier. Due to the random nature of the movements of water vapor molecules, some of them eventually overcome the energy barrier by forming clusters of the new stable phase inside the metastable gas phase. In the context of phase transitions, this process of forming clusters of the stable state inside the metastable parent state is referred to as nucleation. More specifically, two types of nucleation are distinguished: Homogeneous nucleation refers to the process of forming a new, pure cluster of molecules in the stable phase whereas heterogeneous nucleation refers to the formation of a cluster of molecules in the stable phase on or around a cluster of a different molecular species. After a sufficiently large nucleus has formed, it will grow due to the condensation or deposition of water molecules as long as its environment is supersaturated with respect to its phase. Eventually, differences in fall velocities between particles of different sizes will cause them to collide and stick together.
Due to the different molecular properties of water and ice, slightly different processes are involved in the formation of liquid cloud droplets and ice particles. These together with the corresponding growth mechanism are explained in more detail in the following two sections.

2.3 Warm clouds

As mentioned above, warm clouds are clouds that do not extend above the 0 °C-isotherm and consist solely of liquid cloud droplets.

2.3.1 Formation

The formation of cloud droplets by homogeneous nucleation is highly unlikely due to the height of the energy barrier separating the metastable gas phase from the liquid phase. Instead, cloud droplets form through the activation of cloud condensation nuclei (CCN). CCN are soluble aerosol particles, which take up water molecules and grow even in environments that are not super-saturated. The droplets which are formed by hygroscopic growth of aerosol particles are called solution droplets (c.f. Fig. 2.1). For sufficiently high supersaturations, the energy barrier for the transition to larger cloud drops vanishes leading to immediate condensation of all water molecules onto the droplet which are available in its surroundings. The theory describing the activation of CCN and their growth to cloud droplets is known as Köhler theory (Köhler 1936).

2.3.2 Growth processes

The condensation of water molecules onto the newly formed cloud droplet causes a gradient in the concentration of water molecules initiating a diffusive flow of water

vapor towards the droplet. The water vapor flowing towards the droplet condenses onto it causing it to grow in size and mass. This process is called growth by diffusion and condensation. The rate of diffusional growth decreases with increasing droplet radius. For sizes larger than 20 μm it has become so inefficient that another growth process takes over.
When the cloud droplets have grown sufficiently in mass, differences in fall speed between droplets of different size or turbulence may cause droplets to collide. If these droplets coalesce the resulting droplet will have grown compared to the two colliding droplets. The newly-formed larger particle will fall even faster through the cloud. Since heavier particles typically are more efficient in collecting other cloud droplets, this illustrates why collision-coalescence is a very efficient growth process. Only collision-coalescence can explain the onset of rain only 20-30 minutes after the formation of a cumulus cloud which can be observed in the atmosphere (Ch. 7, Lohmann et al. (2016)).

2.4 Cold clouds

Cold clouds extend above 0 °C-isotherm and are characterized by the presence of frozen hydrometeors.

2.4.1 Formation

In contrast to liquid droplets, both homogeneous and heterogeneous nucleation are relevant for the formation of ice particles in the atmosphere. In agreement with Oswald's rule of stages, homogeneous nucleation occurs only through the liquid phase due to the prohibitively high energy barrier associated with the formation of an ice nucleus directly from the vapor phase. This means that ice particles are formed by homogeneous nucleation through the formation of an ice nucleus inside an existing cloud or solution droplet and subsequent complete freezing of the droplet. Nonetheless, the energy barrier for homogeneous nucleation of ice particles remains so high that these processes occur only at temperatures below −36 °C for solution droplets and −38 °C for cloud droplets.
Heterogeneous nucleation of ice particles involves aerosol particles, so called ice nucleating particles (INP), which provide a surface onto which the water molecules can form aggregates with ice-like structure. Heterogeneous nucleation is thought to occur both directly from the gas to the ice phase as well as indirectly through an intermediate liquid phase particle. Heterogeneous freezing, that is heterogeneous nucleation from the liquid phase, occurs when a cloud droplet or a solution droplet comes in contact with an INP upon which the droplet freezes. Heterogeneous freezing may also occur when water vapor condenses directly onto the INP followed by freezing of the liquid nucleus formed on the INP.
Alternatively, heterogeneous nucleation may occur directly from the vapor phase by deposition of water molecules onto the INP. It is, however, still debated whether this process really occurs directly from the vapor phase or whether an intermediate liquid nucleus is formed on the INP.

2.4.2 Growth processes

In principle, the growth processes for ice particles are the same as for liquid droplets. However, due the potential coexistence of particles in the liquid phase these processes have slightly different characteristics as will be explained below.
Due to the lower saturation vapor pressure of ice compared to that of water, a newly-formed ice nucleus experiences a much higher ratio of supersaturation after its formation than a cloud droplet would. This leads to a diffusional growth of ice crystals much faster rates than that of cloud droplets. The rapid growth of the ice particles will deplete the surrounding air of water vapor. This depletion may cause the environment to become sub-saturated with respect to water while it remains saturated with respect to ice. If this is the case, potentially present supercooled cloud droplets evaporate and their molecules deposit onto the ice particles. This is known as the Wegener-Bergeron-Findeisen process.
Similar as for cloud droplets, an ice crystal that grows sufficiently in mass eventually starts to sediment. Size differences between different particles as well as turbulence may cause particles to collide and potentially stick together to form larger particles thus initiating growth by accretion. Accretion is the general term for the growth of hydrometeors caused by the collision of two particles resulting in a permanent union of the two particles. For ice particles, growth by accretion can happen in two ways: The collision of two ice particles, which is called aggregation, or the collision of an ice particle with a liquid particle, which is called riming. Aggregation produces aggregates of snow crystals that, if they don't melt, fall to the ground in the form of snow. Particles produced by riming are known as graupel, when their diameter remains below 2.5 mm, and hail for sizes above that.

2.4.3 Ice habits

Ice crystals exhibit a fascinating range of different forms. Their crystal structure depends on the thermodynamic conditions of their formation. This is because the anisotropic surface tension of a newly formed ice nucleus depends on the temperature and supersaturation.
It is common to distinguish three class of frozen hydrometeors: Pristine ice crystals, aggregates and rimed particles. Common shapes for ice crystals are plates and columns (c.f. Fig 2.1). But also other shapes such as dendrites, stellar plates or needles can be observed. Snow aggregates are usually made up of 10 to 100 or more single crystals. They often consist of dendrites and thin plates. Finally, rimed particles are typically spherical with densities slightly lower than that of solid ice due air inclusions.

2.5 Precipitation

Precipitation occurs when the hydrometeors inside a cloud have grown sufficiently for their fall speeds to exceed the updraft velocity. Due to the ineffectiveness of diffusional growth for cloud droplets and ice crystals at larger particle sizes, growth

by collision-coalescence and growth by accretion are required to form precipitation at the rates observed in the atmosphere.
The exception to this rule is a phenomenon called cloud-less ice precipitation which refers to ice particles that grow large enough to sediment and reach the ground. This, however, occurs only in very cold climates with clean air such as the Arctic and is therefore not relevant at global scales.
Since the transition between suspended cloud hydrometeors and precipitating hydrometeors is continuous no explicit distinction will be made in the following between the two. Instead ice hydrometeors will be considered as a single species of particles include ice crystals, snowflakes, graupel and hail.

Chapter 3

Microwave radiative transfer in the atmosphere

The underlying physical mechanism that allows cloud and precipitation to be remotely sensed is their interaction with electromagnetic radiation that can be measured from afar using suitable detectors. These interactions are described by the theory of radiative transfer. Since this theory is essential for the understanding and development of retrieval methods, this section provides an introduction to radiative transfer of microwaves in the atmosphere. The focus is put on the interaction of radiation with clouds. This presentation is mostly based on the more comprehensive texts by Mishchenko et al. (2002), Thomas and Stamnes (2002), and Wallace and Hobbs (2006).

3.1 The theory of radiative transfer

Radiative transfer theory describes radiation as monochromatic beams that transport radiant energy through the atmosphere. One of the fundamental quantities of the theory is the spectral intensity I_ν defined as the rate at which a beam consisting of radiation from an infinitesimal frequency interval $d\nu$ centered at ν, with angular extent $d\omega$ and propagating into direction $\hat{\boldsymbol{n}}$, transports energy through an infinitesimal area dA:

$$I_\nu = \frac{d^5 E}{\cos(\theta) dA \; dt \; d\omega \; d\nu} \tag{3.1}$$

where $\cos(\theta)$ is the incidence angle between the surface normal of A and the direction of propagation of the beam. In addition to that, a monochromatic beam of radiation has a polarization state, which describes how the energy flux is split up between the two components of the electric field perpendicular to the propagation direction as well as their respective phase. The intensity of a beam and its polarization state are

described by the Stokes vector

$$\boldsymbol{I} = \begin{bmatrix} I_\nu \\ Q \\ U \\ V \end{bmatrix} \tag{3.2}$$

The four components I_ν, Q, U and V of the Stokes vector fully characterize an electromagnetic plane wave to the extent that it can be measured using traditional detectors. This means that all measurable quantities of the radiation can be derived from the corresponding Stokes vector.
The Stokes vector can be directly related to the electromagnetic field strength of an electromagnetic plane wave allowing it to be derived from the more fundamental theory of electromagnetism. The key advantage of radiative transfer theory, however, is that it allows a simplified treatment of the problems relevant to atmospheric remote sensing which are too complex to be solved by direct application of the laws of electrodynamics.

3.1.1 Interactions with matter

The Stokes vector provides a full description of the radiation measured by any passive remote sensing instrument. To model the radiation reaching the detector, a suitable description how this radiation is created as well as how it changes as it propagates through the atmosphere is required. A common approach in radiative transfer theory is to distinguish three fundamental types of such interactions of radiation with matter: The emission of radiation, its absorption, and the scattering of radiation away from and into its propagation path.

Emission

At temperatures above absolute zero, all matter emits radiation through the process of thermal emission. Thermal emission occurs when matter transitions from a quantum mechanical state of higher energy to one of lower energy which causes the surplus of energy to be emitted in the form of radiation. When considering radiation in the lower atmosphere, the relevant emitters of radiation are the ocean or land surface as well as gas molecules or suspended particles.
A fundamental concept for the description of emission is that of a black body. A black body is a piece of matter that absorbs all incoming radiation. At a given temperature T, the emission of a black body is isotropic and un-polarized. Its spectral intensity is given by Planck's law:

$$B_\nu(\nu, T) = \frac{2h\nu^3}{c^2} \frac{1}{\exp(\frac{h\nu}{k_B T}) - 1} \tag{3.3}$$

where c is the speed of light in the medium, h is the Planck constant and k_B is the Boltzmann constant. The Stokes vector describing the emission from a black body is

given by

$$\boldsymbol{I} = \begin{bmatrix} B_\nu \\ 0 \\ 0 \\ 0 \end{bmatrix}. \tag{3.4}$$

The concept of the black body is used to define the emission from other forms of matter using the emissivity vector $\boldsymbol{\epsilon}$:

$$\boldsymbol{I} = \boldsymbol{\epsilon} \cdot B_\nu \tag{3.5}$$

The main difference between the treatment of emission from a volume compared to that of a surface is the unit of the emission vector $\boldsymbol{\epsilon}$. For a volume, it is defined per unit length of the path through the volume, while for a surface this is not necessary. Due to the distinct orientation that surfaces have with respect to the viewing geometry, the emissivity vector generally depends on the emission angle. For particles this is generally also the case, but since most particles in the atmosphere are randomly oriented it is often neglected. Although black-body radiation is unpolarized, emission from general emitters can be polarized. An important example is the ocean surface, which is highly polarized around the Brewster angle at 53°.

Absorption

Absorption refers to the process of radiation being converted into internal energy of the matter it interacts with. Mathematically, this process is described by the absorption vector $\boldsymbol{\alpha}$, defined as the fraction of the incoming radiation that is absorbed along an infinitesimal distance ds along the propagation path:

$$\boldsymbol{I}_{\text{absorbed}} = (\boldsymbol{\alpha} \cdot \ ds) \odot \boldsymbol{I} \tag{3.6}$$

Here $\odot$ denotes the element-wise product of the absorption vector and the Stokes vector $\boldsymbol{I}$ of the incoming radiation. Absorption may be understood as the inverse process of thermal emission. Formally, this is expressed by Kirhoff's law of radiation

$$\boldsymbol{\alpha} = \boldsymbol{\epsilon}, \tag{3.7}$$

which states that the absorption vector is identical to the emissivity vector defined in Eq. 3.5. This law is applicable to all matter in the atmosphere given that it is in a state of local thermal equilibrium (LTE). LTE occurs when the density of matter is sufficiently high so that the population rates of energy states above the ground state are determined by thermal collisions rather than the absorption of radiation. This decouples the emission of radiation from the radiation field, allowing the simplified treatment of matter as thermal emitters with the emission rates independent of the radiation field. LTE is a valid assumption for radiative transfer in the lower atmosphere.

Scattering

When a beam of radiation impinges upon a particle, their interaction may cause a deviation of parts of the beam from the original propagation path. To first order, scattering decreases the intensity of the beam. This particular process is referred to as single scattering. As it propagates through the atmosphere, the intensity of a beam is decreased by the effects of absorption and single scattering. The combination of these two processes is referred to as attenuation or extinction. As the rate of scattering increases, also the effect radiation that is being scattered into the beam has to be taken into account.
Mathematically, the scattering of a beam of light propagating in direction $\boldsymbol{n}$ into the direction $\hat{\boldsymbol{n}}$ is described by the phase matrix $\boldsymbol{Z}(\hat{\boldsymbol{n}}, \boldsymbol{n})$:

$$\boldsymbol{I}_{\text{scattered}}(\hat{\boldsymbol{n}}) = \boldsymbol{Z}(\hat{\boldsymbol{n}}, \boldsymbol{n})\boldsymbol{I}(\boldsymbol{n}) \tag{3.8}$$

The combined, attenuating effects of scattering and absorption are given by the attenuation matrix $\boldsymbol{K}$, which is the sum of the absorption vector $\boldsymbol{\alpha}$ and the fraction of radiation scattered away from the propagation path:

$$\boldsymbol{K} = \begin{bmatrix} | & | & | & | \\ \boldsymbol{\alpha} & \mathbf{0} & \mathbf{0} & \mathbf{0} \\ | & | & | & | \end{bmatrix} + \int_{\hat{\boldsymbol{n}}} d\hat{\boldsymbol{n}}\ \boldsymbol{Z}(\hat{\boldsymbol{n}}, \boldsymbol{n}) \tag{3.9}$$

3.1.2 The radiative transfer equation

The previous section introduced the fundamental interactions of radiation with matter and how they are described mathematically in radiative transfer theory. Combining the three processes of emission, absorption and scattering, the change that a beam undergoes as it travels a distance ds along its propagation path through the atmosphere is described the vector radiative transfer equation (VRTE):

$$\frac{d\boldsymbol{I}(\boldsymbol{n})}{ds} = -\boldsymbol{K}\boldsymbol{I}(\boldsymbol{n}) + \boldsymbol{\alpha} \cdot B_\nu(T) + \int_{\hat{\boldsymbol{n}}} d\hat{\boldsymbol{n}}\ \mathbf{Z}(\boldsymbol{n}, \hat{\boldsymbol{n}})\boldsymbol{I}(\hat{\boldsymbol{n}}). \tag{3.10}$$

The radiation field for an arbitrary atmosphere can be computed by solving Equation (3.10). What is required for this are the values of temperature, absorption vector $\boldsymbol{\alpha}$ and phase matrices $\boldsymbol{Z}$ throughout the atmosphere as well as a suitable method for solving the radiative transfer equation. The values of $\boldsymbol{\alpha}$ and $\boldsymbol{Z}$ describe how a specific volume element of the atmosphere absorbs and scatters radiation. Their values therefore depend on the concentrations of gases and particulate matter in the atmosphere.
Approximate values of $\boldsymbol{\alpha}$ and $\boldsymbol{Z}$ for different materials in the atmosphere can be measured experimentally or in special cases even derived from first principles. Typically they depend on local properties of the atmosphere such as temperature, pressure or concentration of gases or particles. Numerical models for $\boldsymbol{\alpha}$ and $\boldsymbol{Z}$ together with the VRTE thus allow the radiation field observed by remote sensing intruments to be related to the state of the atmosphere. Together with the methods described in Section 4, this forms the basis of atmospheric remote sensing.

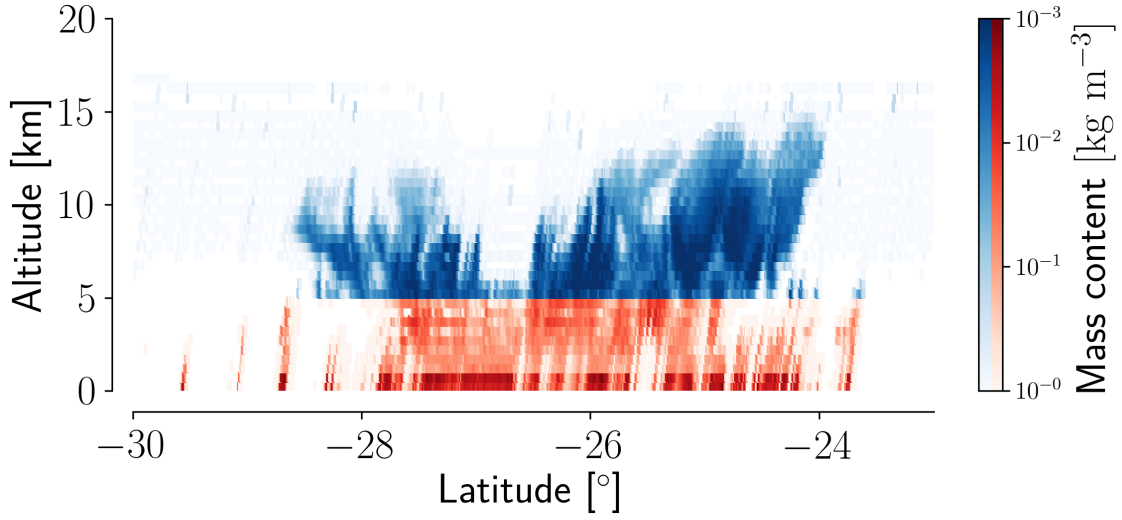

Figure 3.1: Mass content of frozen (blue) and liquid hydrometeors retrieved from the radar reflectivities show in Fig. 1.2

3.2 Microwave observations of clouds and precipitation

To illustrate the application of radiative transfer theory to observations of clouds and precipitation, we now turn back to the example cloud scene considered in Sec. 1.3. A simple hydrometeor retrieval has been performed to estimate the mass concentrations of frozen and liquid hydrometeors in the observed cloud using the radar observations displayed in Fig. 1.2. For simplicity, it was assumed that all hydrometeors below (in altitude) the 0 °C-isotherm are in the liquid phase and the ones above in the ice phase. The retrieved mass concentrations are displayed in Fig. 3.1. Since a standard tropical atmosphere has been assumed to retrieve the cloud properties, the melting layer and hence the boundary between liquid and ice hydrometeors is at a constant altitude across the whole scene. Although this is certainly not a very accurate assumption especially since the radar reflectivities show signs of convective activity, it is sufficient to illustrate the basic interaction of microwave radiation with clouds and precipitation. The simplified cloud model obtained in this way is can now by used to simulate the signatures of liquid and frozen hydrometeors in the passive microwave observations.

3.2.1 Liquid hydrometeors

We start by investigating the effect of liquid hydrometeors on passive microwave observations. For this, all frozen hydrometeors in the scene are ignored and observations are simulated of the four passive microwave frequencies considered in Fig. 1.2. The results of these simulations are displayed in Fig. 3.2. Shown is the signal from clouds and precipitation defined as the difference in the simulated microwave signal

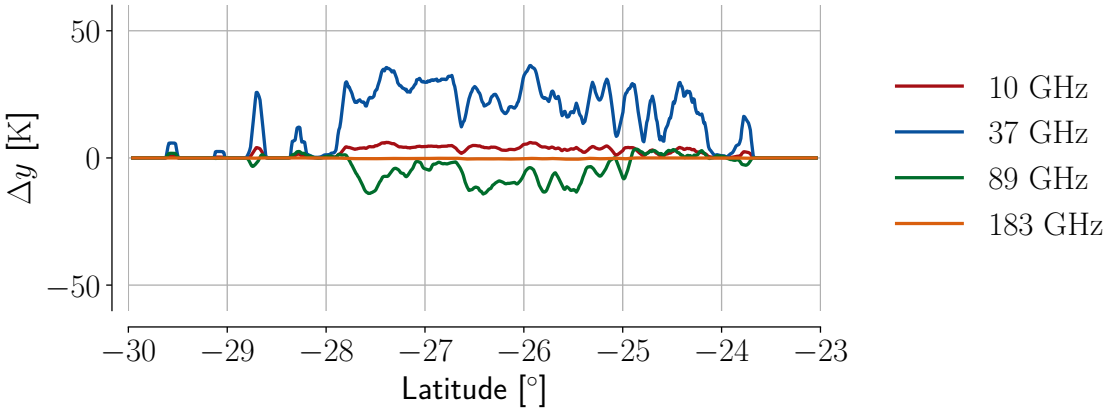

Figure 3.2: Simulated differences in observed passive radiances with respect to a cloud-free reference observation Δy for different microwave frequencies when only liquid hydrometeors are considered.

with respect to a cloud-free reference observation:

$$\Delta y = y_{\text{cloudy}} - y_{\text{clear}} \tag{3.11}$$

At frequencies as low as 10 GHz, the signal observed from the rain is positive. At these frequencies, rain drops interact with radiation mostly through absorption. Above the sea surface, which acts as a cold background, the rain is therefore observed as a warm signal. At 37 GHz, an even stronger positive signal is observed from the precipitation. The increase in the strength of the signal is due to the increased absorption at shorter wavelengths. As the frequency is increased to 89 GHz, the precipitation signal switches sign from positive to negative. This is because the sensitivity to water vapor causes the background to become warmer, while at the same time the rain drops become more effective scatters. The observed rain signal is therefore due to radiation that is being scattered away from the line of sight by the rain drops, leading to a negative signal.
At 183 GHz, finally, the precipitation signal has fully disappeared. This is because these frequencies the sensitivity to water vapor is so high that the sensor is essentially blind to the lower parts of the troposphere in which the rain is located.

3.2.2 Frozen hydrometeors

To now assess the additional effects of frozen hydrometeors, the simulations are run once again but this time including also the frozen hydrometeors in the simulations. The resulting cloud signals are displayed in Fig. 3.3.
First of all, it can be noticed that the precipitations signals observed at 10 GHz and 37 GHz are not affected by the presence of frozen hydrometeors. Although frozen precipitating particles are of similar sizes as rain drops, differences in their dielectric constants cause the ice to interact less strongly with the radiation than water. At 89 and 183 GHz, however, a clear negative signal from the ice particles is observed. At 183 GHz, all of the observed cloud signal is due to the scattering from frozen hydrometeors.

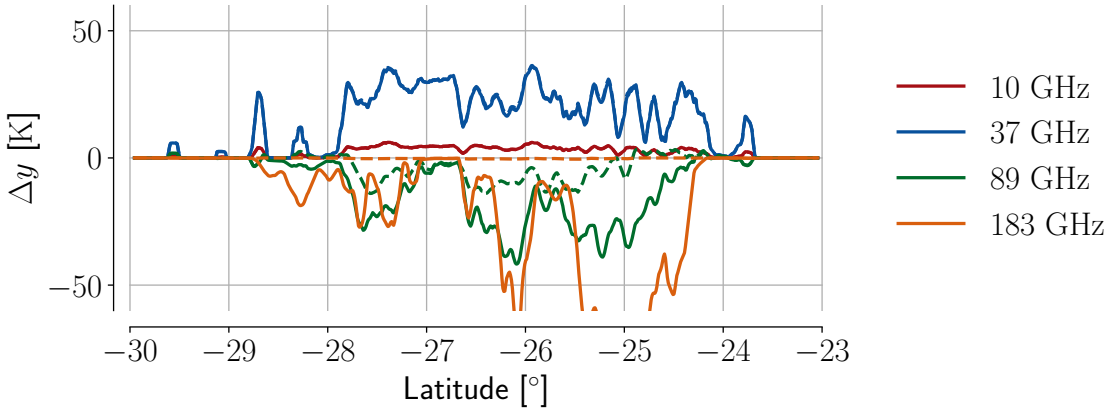

Figure 3.3: Simulated differences in observed passive radiances with respect to a cloud-free reference observation Δy when both liquid and frozen hydrometeors are considered. Dashed lines show the corresponding signal due to rain only (c.f. Fig. 3.2).

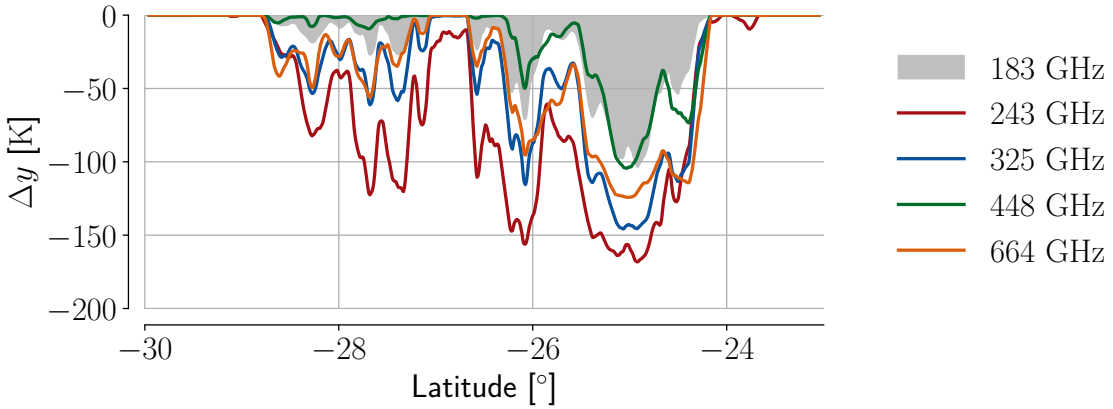

Figure 3.4: Signature of clouds in microwave observations. The plot shows the simulated cloud signal as it would be observed by the reference observation when both liquid and frozen hydrometeors are considered.

3.2.3 Sub-millimeter wavelengths

Finally, the simple cloud model can be used to demonstrate the benefits of sub-millimeter wavelengths for cloud observations. For this, we consider the cloud signal observed by four of the channels of the upcoming ICI instrument located at $248, 325, 448$ and 664 GHz. The simulated cloud signals are displayed in Fig. 3.4. The cloud signal in all of the considered channels is considerably stronger than that at 183 GHz. In particular in the left part of the scene, the cloud signals at sub-millimeter wavelength are significantly stronger than that observed at 183 GHz. Since observations at 183 GHz are sensitive only to particles large enough to be considered snow, the signal observed here indicates the presence ice clouds. This shows that ICI will bring immense benefits for observations of clouds using microwave radiation.

Chapter 4

Inverse problems

The previous chapters provided an overview over the general properties of clouds and their interaction with electromagnetic radiation which is used to observe them. This chapter describes the mathematical methods that are used to infer properties of clouds from their signatures in the observed electromagnetic radiation. Mathematically, this task is formulated as an inverse problem. This is because inferring the cloud properties from observations can be viewed as the inverse of the problem of predicting the observations given the cloud properties, which is referred to as the forward problem. How the forward problem can be solved using radiative transfer theory has been described in the previous chapter. In this chapter we now turn to the task of solving the inverse problem.

4.1 Formulation

Mathematically, the general inverse problem of remote sensing is formulated as follows: Let $\boldsymbol{x} \in \mathbb{R}^n$ be an arbitrary vector that describes the state of the atmosphere. The vector space of all possible states is referred to as the state space and for simplicity assumed to be given by $\mathbb{R}^n$. The state atmospheric state $\boldsymbol{x}$ is observed through an observations system, which produces the observation vector $\boldsymbol{y} \in \mathbb{R}^m$. Furthermore, it is assumed here that a forward model $\mathbf{F} : \mathbb{R}^n \to \mathbb{R}^m$ exists that allows computing the observation $\boldsymbol{y} = \mathbf{F}(\boldsymbol{x})$ corresponding to any given state vector $\boldsymbol{x}$. The inverse problem consists of determining the state vector $\boldsymbol{x}$ corresponding to a given the observation vector $\boldsymbol{y}$, hence to invert the forward model $\mathbf{F}$.
The general difficulty with inverse problems is that they do not admit a unique solution. This is because, at least in atmospheric remote sensing, the problem is generally underconstrained. This means that the amount of information in the observations $\mathbf{y}$ is not sufficient to uniquely determine a state $\mathbf{x}$. Examples are different cloud configurations that result in the same measurement vector such as for example a low-level cloud covered by an opaque high-level cloud. From the measurement vector $\boldsymbol{y}$ alone it is impossible to determine a unique state $\boldsymbol{x}$ as it will be the same independent of the presence or properties of the low-level cloud.
Simultaneously to being underconstrained, the problem may be overconstrained. This happens when different components of the measurement vector provide seemingly

contradictory information on the measurement state $\boldsymbol{x}$ due errors random errors in $\boldsymbol{y}$.

4.2 Solution

A common approach in atmospheric remote sensing to solve inverse problems is the application of Bayesian statistics. This means that instead of searching a unique solution to the inverse problem, the solution is found in the form of a probability distribution that describes how likely it is that any of the elements of the state space has produced a given observation $\boldsymbol{y}$.
The approach that will be presented in the following is known as the optimal estimation method (OEM, Rodgers (2000)). The method makes three basic assumptions in order to solve the inverse problem:

1. That the forward model $\mathbf{F}$ is linear or at most weakly non-linear,
2. that the knowledge available about $\boldsymbol{x}$ can be described by a Gaussian distribution, with mean $\boldsymbol{x}_a$ and covariance matrix $\boldsymbol{S}_a^{-1}$
3. that the errors affecting $\mathbf{y}$ are Gaussian with covariance matrix $\boldsymbol{S}_\epsilon$.

Under these assumptions, both the a priori distribution for $\boldsymbol{x}$ as well as the conditional probability of observing the measurement $\boldsymbol{y}$ given the state $\boldsymbol{x}$ are Gaussian:

$$p(\boldsymbol{x}) = \frac{1}{(2\pi)^{\frac{-n}{2}}\det(\boldsymbol{S}_a)^{-\frac{1}{2}}} \exp\left\{-\frac{1}{2}(\boldsymbol{x}-\boldsymbol{x}_a)^T\boldsymbol{S}_a^{-1}(\boldsymbol{x}-\boldsymbol{x}_a)\right\} \tag{4.1}$$

$$p(\boldsymbol{y}|\boldsymbol{x}) = \frac{1}{(2\pi)^{\frac{-m}{2}}\det(\boldsymbol{S}_e)^{-\frac{1}{2}}} \exp\left\{-\frac{1}{2}(\boldsymbol{x}-\mathbf{F}(\boldsymbol{x}))^T\boldsymbol{S}_e^{-1}(\boldsymbol{x}-\mathbf{F}(x))\right\} \tag{4.2}$$

In the Bayesian framework the solution of the inverse problem is simply the a posteriori distribution $p(\boldsymbol{x}|\boldsymbol{y})$ of $\boldsymbol{x}$ given the observation vector $\boldsymbol{y}$. It is found by applying Bayes theorem

$$p(\boldsymbol{y}|\boldsymbol{x}) = \frac{p(\boldsymbol{y}|\boldsymbol{x})p(\boldsymbol{x})}{p(\mathbf{y})} \tag{4.3}$$

$$\propto p(\boldsymbol{y}|\boldsymbol{x})p(\boldsymbol{x}) \tag{4.4}$$

to the probabilities (4.1) and (4.2).
As a specific solution of the retrieval problem, generally the most likely state is chosen, denoted as the maximum a posteriori (MAP) estimator for $\boldsymbol{x}$. It can be found by minimizing the log-likelihood of the posterior distribution, which has the form:

$$-\mathcal{L} \propto (\boldsymbol{F}(\boldsymbol{x})-\boldsymbol{y})^T\boldsymbol{S}_\epsilon^{-1}(\boldsymbol{F}(\boldsymbol{x})-\boldsymbol{y}) + (\boldsymbol{x}-\boldsymbol{x}_a)^T\boldsymbol{S}_a^{-1}(\boldsymbol{x}-\boldsymbol{x}_a) \tag{4.5}$$

Solving the retrieval problem has thus been reduced to minimizing the negative log-likelihood of the posterior distribution. When the forward model is non-linear, minimizing Eq. (4.5) must be performed iteratively using suitable optimization methods such as the Gauss-Newton or Levenberg-Marquardt methods (Boyd and Vandenberghe 2004).

4.3 Error estimation

A major advantage of the OEM formalism is that it allows precise characterization of the errors that affect the retrieved state. Given below is a derivation of the retrieval error from the formulation of the OEM for a linear forward model and in the absence of forward model errors. How these results can be generalized to a non-linear forward model and the presence of forward modeling errors are outlined afterwards.

4.3.1 The idealized case

We start by defining a retrieval operator $\hat{\boldsymbol{x}} = \mathbf{R}(\boldsymbol{y})$ which represents the application of the retrieval to an observation vector $\boldsymbol{y}$ yielding the retrieved state $\hat{\boldsymbol{x}}$. If the forward model is assumed to be exact, then $\boldsymbol{y}$ can be written as the sum of the forward model evaluated at the true state $\boldsymbol{x}$ and a random vector of measurement noise:

$$\mathbf{y} = \mathbf{F}(\boldsymbol{x}) + \boldsymbol{\epsilon}. \tag{4.6}$$

Inserting this into $\mathbf{R}$ and linearizing the forward model $\mathbf{F}$ about the a priori state $\boldsymbol{x}_a$ yields

$$\mathbf{R}(\boldsymbol{y}) = \mathbf{R}\left(\mathbf{F}(\boldsymbol{x}_a) + \mathbf{K}(\boldsymbol{x} - \boldsymbol{x}_a) + \boldsymbol{\epsilon}\right), \tag{4.7}$$

where $\boldsymbol{K} = \frac{d\boldsymbol{F}}{d\boldsymbol{x}}$ is the Jacobian of the forward model. Now, linearizing the retrieval operator about $\mathbf{y}$ allows us to write

$$\hat{\boldsymbol{x}} = \mathbf{R}(\mathbf{F}(\boldsymbol{x}_a)) + \frac{d\mathbf{R}}{d\boldsymbol{x}}\mathbf{K}(\boldsymbol{x} - \boldsymbol{x}_a) + \frac{d\mathbf{R}}{d\boldsymbol{x}}\epsilon. \tag{4.8}$$

Assuming an unbiased retrieval operator, i.e. $\mathbf{R}(\boldsymbol{F}(\boldsymbol{x})) - \boldsymbol{x}_a = 0$, the retrieved information on the state $\boldsymbol{x}$ may be written as

$$\hat{\boldsymbol{x}} - \boldsymbol{x}_a = \frac{d\mathbf{R}}{d\boldsymbol{x}}\mathbf{K}(\boldsymbol{x} - \boldsymbol{x}_a) + \frac{d\mathbf{R}}{d\boldsymbol{x}}\epsilon. \tag{4.9}$$

The derivative of the retrieval operator $\mathbf{R}$ with respect to the observation vector $\mathbf{y}$ is referred to as the gain matrix $\mathbf{G}$ and is found to be given by

$$\mathbf{G} = (\boldsymbol{K}^T\boldsymbol{S}_\epsilon^{-1}\boldsymbol{K} + \boldsymbol{S}_a^{-1})^{-1}\boldsymbol{K}^T\boldsymbol{S}_\epsilon^{-1}. \tag{4.10}$$

We further define the so-called averaging kernel matrix $\mathbf{A} = \mathbf{GK}$. With this, the retrieval error can be written as

$$\hat{\boldsymbol{x}} - \boldsymbol{x} = \underbrace{(\mathbf{A} - \boldsymbol{I})(\boldsymbol{x} - \boldsymbol{x}_a)}_{\text{Smoothing error}} + \underbrace{\frac{d\mathbf{R}}{d\boldsymbol{x}}\epsilon}_{\text{Error due to noise}}. \tag{4.11}$$

This shows that the retrieval error can be written as the sum of two contributions. The first term on the right hand side is the so called smoothing error. It can be

interpreted as the retrieval error that occurs because of the limited resolution of the observation system. Its covariance matrix is given by

$$\boldsymbol{S}_s = (\boldsymbol{A} - \boldsymbol{I})\boldsymbol{S}_\epsilon(\boldsymbol{A} - \boldsymbol{I}). \tag{4.12}$$

The second term on the right-hand side of Eq. (4.11) is the error caused by the noise in the observations. Its covariance matrix is given by

$$\boldsymbol{S}_m = \boldsymbol{G}_y\boldsymbol{S}_\epsilon\boldsymbol{G}_y^T. \tag{4.13}$$

4.3.2 Handling forward model error and non-linearity

The derivation presented above assumed an ideal forward model, which is of course rarely the case in reality. It is possible to generalize the formulation of the retrieval error, if the forward model error can be assumed to be bias free and described using a Gaussian distribution with covariance matrix $\boldsymbol{S}_e$. In this case the general retrieval error can be obtained by simply replacing $\boldsymbol{S}_\epsilon$ in Eq. (4.13) with $\boldsymbol{S}_\epsilon + \boldsymbol{S}_e$.
If the forward model in non-linear, the forward model in the above derivation has to be linearized about the most recent state in the retrieval iteration $\boldsymbol{x}_i$. In this case the bias term $\mathbf{R}(\boldsymbol{F}(\boldsymbol{x}_i)) - \boldsymbol{x}_a$ can no longer be assumed to be zero, and the retrieval results will become biased.

Chapter 5

Summary of appended papers and outlook

After introducing the physical and mathematical principles of the remote sensing of clouds, this chapter now turns towards the research that has been carried out under the general aim of preparations for the upcoming ICI sensor. The two scientific articles appended to this thesis investigate the concept of combining radar and radiometer observations for retrieving ice hydrometeors. The studies were carried out within the context of the study "Scientific Concept Study for Wide-Swath High-Resolution Cloud Profiling" funded by the European Space Agency which investigated the potential benefits of a hypothetical cloud radar mission flying in constellation with ICI to provide co-located radar and sub-millimeter radiometer observations.

5.1 Paper A: Synergistic radar and radiometer retrievals of ice hydrometeors

A synergistic retrieval algorithm is proposed which uses the OEM to retrieve ice hydrometeors from combined radar and sub-millimeter radiometer observations. The study aims to establish the fundamental synergies of the combined observations, i.e. the additional information that can be gained from the observations when they are used simultaneously in the retrieval instead of considering them separately.

5.1.1 Data and methods

The study uses simulated observations from a high-resolution atmospheric model to produce synthetic, co-located observations from a cloud radar and a sub-millimeter radiometer. By applying the retrieval to these synthetic observations its performance is assessed. The combined retrieval is compared to radar-only and passive-only versions of the retrieval algorithm to establish the advantages of the synergistic retrieval approach.

5.1.2 Results

The results obtained in this study show the combination of radar and radiometer observations helps to better constrain the microphysical properties of clouds. The increased sensitivity to microphysical properties of the cloud reduces uncertainties in retrieved ice mass concentrations. In addition to that, the combined retrieval showed improved skill in the detection and retrieval of liquid clouds.

5.1.3 Conclusions

The increased information content of the combined observations allows an additional degree of freedom of the distribution of ice hydrometeors to be retrieved, which helps to reduce uncertainties in the retrieved ice mass concentrations. This information gain could be attributed to the sub-millimeter channels of the ICI sensor. It is therefore concluded that combined retrievals involving radar and sub-millimeter radiometer observations are a promising approach that may help to reduce uncertainties in retrievals of frozen hydrometeors.

5.2 Paper B: Relating microphysical and radiometric properties of cloud hydrometeors at millimeter and sub-millimeter wavelengths

The second paper builds upon the first one by applying the synergistic retrieval algorithm to observations from a recent flight campaign. One of the few currently available sensors that can produce ICI-type sub-millimeter observations of clouds is the International Submillimetre Airborne Radiometer (ISMAR, Fox et al. (2017)), which serves as the airborne demonstrator for the ICI sensor. In 2016, ISMAR took part in a joint flight campaign in which three research aircraft performed a simultaneous overpass of a mid-latitude cloud system and observed it using a wide range of remote sensing sensors. Since cloud radars were present on the other two aircraft, the observations made during the campaign provide a unique opportunity to apply and test the synergistic retrieval algorithm.

5.2.1 Data and method

The study uses observations acquired by the joint flight of the High Altitude and Long Range Research Aircraft (HALO), the Facility for Airborne Atmospheric Measurements (FAAM) and the Service des Avions Francais Instrumentions pour la Recherche en Environnement (SAFIRE) research aircraft. The data consists of remote sensing observations from the overpass and in-situ data collected by the FAAM aircraft.

The in-situ data available from the flight are used to characterize the microphysical properties of the hydrometeors in the observed cloud. Since assumption on these

properties affect the results of the retrieval, this characterization is necessary for their analysis.
Following this, the synergistic retrieval algorithm is applied to the observations from the flight. The fits of the forward model to the observations are evaluated to check the consistency of the radiative transfer modeling upon which the retrieval is based. The retrieved hydrometeor profiles are compared to those derived from the in-situ data. Finally, the consistency of the retrieved hydrometeor distributions with the other observations from the flight is assessed by comparing them to simulations obtained from the retrieval results.

5.2.2 Results

An important result of this study is that the retrieval does achieve a good fit to the observations over large parts of the scene, which shows that the applied radiative transfer scheme is able to consistently model the observations over the wide range of microwave frequencies that was considered here. Two regions in which the retrieval does not fit the observations show signs of convective activity indicating the presence of a signal from the specific microphysical properties of the hydrometeors in the updraft.
Although dependent on the employed particle model, the retrieval results show generally good agreement with the in-situ measurements. This dependency, however, is found to be consistent with the microphysical characterization derived from the in-situ measurements, which speaks in favor of the validity of the retrieval method. Moreover, the simulated observations of an additional radar operating at a different frequency show good agreement with the real observations.

5.2.3 Conclusions

The results presented in this study validate the implementation of the developed synergistic retrieval algorithm and thus confirm the results from the first study. Moreover, the good fit to the observations obtained in the retrieval demonstrates the consistency of the radiative transfer modeling through clouds at millimeter and sub-millimeter wavelengths. The results therefore provide an important validation case for the modeling of radiative transfer at sub-millimeter wavelengths.

5.3 Outlook

5.3.1 Relevance of the results

The focus of the presented research were combined retrievals using radar and sub-millimeter radiometer observations. Since such observation are currently not available from any ongoing satellite missions, this research is relevant to prospective satellite missions involving radar and sub-millimeter observations. In addition to that, the second study demonstrated the usefulness of the approach also for the application in

field campaigns where it may be used to validate the radiative transfer modeling of clouds and possibly even to study their microphysical properties.
The presented results also have a more general relevance with respect to the upcoming ICI mission. Since currently available sub-millimeter observations of clouds are limited, the radiative transfer modeling at these frequencies is still afflicted with considerable uncertainties. These uncertainties will need to be addressed in order to put the observations from ICI to proper use. The application of the combined retrieval described in Paper B validated the radiative transfer modeling at sub-millimeter wavelengths but also highlighted remaining modeling issues regarding the properties of hydrometeors in regions of strong convective activity.

5.3.2 Future work

Although the presented work established the basic consistency of radiative transfer modeling of clouds at sub-millimeter wavelengths, there remain a number of challenges that should be addressed. One of them is certainly the representation of the ice particles in radiative transfer simulations at sub-millimeter wavelengths. This could be further investigated by making use of other field campaigns involving the ISMAR radiometer. Alternatively, co-locations of currently available satellite observations could be used as has been attempted in ekelund19. This work could be further extended by including infrared observations and by using directly co-located observations such as the ones shown in Sec. 1.3.
A more specific line of future work that arises from the results of the second study is to investigate the radiometric properties of hydrometeors in convective updrafts. The observations from the flight campaign could serve as a case study to establish the basic radiometric properties of the hydrometeors present in these updrafts. These could then be used to investigate the effect of the derived properties on already available microwave observations of clouds.
Finally, since the ability to model the radiative transfer at sub-millimeter wavelengths is the foundation for understanding and making use of the observations that will be provided by ICI, the general consolidation of radiative transfer models at sub-millimeter wavelengths remains an essential issue. An important resource for this are the air-borne observations from the ISMAR sensor, which should be used for continued validation studies for the radiative transfer modeling at these wavelengths.

Bibliography

Bony, S., B. Stevens, D. M. Frierson, C. Jakob, M. Kageyama, R. Pincus, T. G. Shepherd, S. C. Sherwood, A. P. Siebesma, A. H. Sobel, et al. (2015). "Clouds, circulation and climate sensitivity". In: *Nat. Geosci.* 8.4, p. 261 (cit. on p. 5).

Boucher, O., D. Randall, P. Artaxo, C. Bretherton, G. Feingold, P. Forster, V.-M. Kerminen, Y. Kondo, H. Liao, U. Lohmann, P. Rasch, S. Satheesh, S. Sherwood, B. Stevens, and X. Zhang (2013). "Clouds and Aerosols". In: *Climate Change 2013: The Physical Science Basis. Contribution of Working Group I to the Fifth Assessment Report of the Intergovernmental Panel on Climate Change*. Ed. by T. Stocker, D. Qin, G.-K. Plattner, M. Tignor, S. Allen, J. Boschung, A. Nauels, Y. Xia, V. Bex, and P. Midgley. Cambridge, United Kingdom and New York, NY, USA: Cambridge University Press. Chap. 7, pp. 571–658. ISBN: ISBN 978-1-107-66182-0. DOI: 10.1017/CBO9781107415324.016 (cit. on p. 5).

Boyd, S. and L. Vandenberghe (2004). *Convex optimization*. Cambridge university press (cit. on p. 26).

Buehler, S., E. Defer, F. Evans, S. Eliasson, J. Mendrok, P. Eriksson, C. Lee, C. Jiménez, C. Prigent, S. Crewell, et al. (2012). "Observing ice clouds in the submillimeter spectral range: the CloudIce mission proposal for ESA's Earth Explorer 8". In: *Atmos. Meas. Tech.* 5.7, pp. 1529–1549 (cit. on p. 8).

Collins, M., R. Knutti, J. Arblaster, J.-L. Dufresne, T. Fichefet, P. Friedlingstein, X. Gao, W. Gutowski, T. Johns, G. Krinner, M. Shongwe, C. Tebaldi, A. Weaver, and M. Wehner (2013). "Long-term Climate Change: Projections, Commitments and Irreversibility". In: *Climate Change 2013: The Physical Science Basis. Contribution of Working Group I to the Fifth Assessment Report of the Intergovernmental Panel on Climate Change*. Ed. by T. Stocker, D. Qin, G.-K. Plattner, M. Tignor, S. Allen, J. Boschung, A. Nauels, Y. Xia, V. Bex, and P. Midgley. Cambridge, United Kingdom and New York, NY, USA: Cambridge University Press. Chap. 12, pp. 1029–1136. ISBN: ISBN 978-1-107-66182-0. DOI: 10.1017/CBO9781107415324.024 (cit. on p. 3).

Coronese, M., F. Lamperti, K. Keller, F. Chiaromonte, and A. Roventini (2019). "Evidence for sharp increase in the economic damages of extreme natural disasters". In: *Proceedings of the National Academy of Sciences* 116.43, pp. 21450–21455. ISSN: 0027-8424. DOI: 10.1073/pnas.1907826116 (cit. on p. 3).

Draper, D. W., N. D. A., F. J. Wentz, S. Krimchansky, and G. M. Skofronick-Jackson (2015). "The Global Precipitation Measurement (GPM) Microwave Imager (GMI): Instrument Overview and Early On-Orbit Performance". In: *IEEE Journal of*

Selected Topics in Applied Earth Observations and Remote Sensing 8.7, pp. 3452–3462. ISSN: 2151-1535. DOI: 10.1109/JSTARS.2015.2403303 (cit. on p. 7).

Fox, S., C. Lee, B. Moyna, M. Philipp, I. Rule, S. Rogers, R. King, M. Oldfield, S. Rea, M. Henry, H. Wang, and R. C. Harlow (2017). "ISMAR: an airborne submillimetre radiometer". In: *Atmos. Meas. Tech.* 10.2, pp. 477–490. DOI: 10.5194/amt-10-477-2017 (cit. on p. 30).

Geer, A. J., F. Baordo, N. Bormann, P. Chambon, S. J. English, M. Kazumori, H. Lawrence, P. Lean, K. Lonitz, and C. Lupu (2017). "The growing impact of satellite observations sensitive to humidity, cloud and precipitation". In: *Q. J. R. Meteorol. Soc.* 143.709, pp. 3189–3206. DOI: 10.1002/qj.3172 (cit. on p. 4).

Geer, A. J., K. Lonitz, P. Weston, M. Kazumori, K. Okamoto, Y. Zhu, E. H. Liu, A. Collard, W. Bell, S. Migliorini, P. Chambon, N. Fourrié, M.-J. Kim, C. Köpken-Watts, and C. Schraff (2018). "All-sky satellite data assimilation at operational weather forecasting centres". In: *Q. J. R. Meteorol. Soc.* 144.713, pp. 1191–1217. DOI: 10.1002/qj.3202 (cit. on p. 4).

Grinsted, A., P. Ditlevsen, and J. H. Christensen (2019). "Normalized US hurricane damage estimates using area of total destruction, 1900-2018". In: *Proceedings of the National Academy of Sciences*. ISSN: 0027-8424. DOI: 10.1073/pnas.1912277116 (cit. on p. 3).

Hellmann, G. (1908). "The dawn of meteorology". In: *Quarterly Journal of the Royal Meteorological Society* 34.148, pp. 221–232. DOI: 10.1002/qj.49703414802 (cit. on p. 3).

Köhler, H. (1936). "The nucleus in and the growth of hygroscopic droplets". In: *Transactions of the Faraday Society* 32, pp. 1152–1161 (cit. on p. 13).

Lohmann, U., F. Lüönd, and F. Mahrt (2016). *An introduction to clouds: From the microscale to climate*. Cambridge University Press (cit. on pp. 11, 12, 14).

Masson-Delmotte, V., M. Schulz, A. Abe-Ouchi, J. Beer, A. Ganopolski, J. González Rouco, E. Jansen, K. Lambeck, J. Luterbacher, T. Naish, T. Osborn, B. Otto-Bliesner, T. Quinn, R. Ramesh, M. Rojas, X. Shao, and A. Timmermann (2013). "Information from Paleoclimate Archives". In: *Climate Change 2013: The Physical Science Basis. Contribution of Working Group I to the Fifth Assessment Report of the Intergovernmental Panel on Climate Change*. Ed. by T. Stocker, D. Qin, G.-K. Plattner, M. Tignor, S. Allen, J. Boschung, A. Nauels, Y. Xia, V. Bex, and P. Midgley. Cambridge, United Kingdom and New York, NY, USA: Cambridge University Press. Chap. 5, pp. 383–464. ISBN: ISBN 978-1-107-66182-0. DOI: 10.1017/CBO9781107415324.013 (cit. on p. 3).

Mishchenko, M. I., L. D. Travis, and A. A. Lacis (2002). *Scattering, absorption, and emission of light by small particles*. Cambridge university press (cit. on p. 17).

Rodgers, C. D. (2000). *Inverse methods for atmospheric sounding: theory and practice*. Vol. 2. World scientific (cit. on p. 26).

Tanelli, S., S. L. Durden, E. Im, K. S. Pak, D. G. Reinke, P. Partain, J. M. Haynes, and R. T. Marchand (2008). "CloudSat's Cloud Profiling Radar After Two Years in Orbit: Performance, Calibration, and Processing". In: *IEEE T. Geosci. Remote* 46.11, pp. 3560–3573. ISSN: 0196-2892. DOI: 10.1109/TGRS.2008.2002030 (cit. on p. 8).

Thomas, G. E. and K. Stamnes (2002). *Radiative transfer in the atmosphere and ocean*. Cambridge University Press (cit. on p. 17).

Wallace, J. M. and P. V. Hobbs (2006). *Atmospheric science: an introductory survey*. Vol. 92. Elsevier (cit. on p. 17).